Inorg. Chem. **2003**, *42*, 5392–5398

X-ray Absorption Spectroscopic Studies of Chromium Nitroso Complexes. Crystal and Molecular Structure of $(Ph_4P)_3[Cr(NO)(NCS)_5]\cdot 2.4(CH_3)_2CO$

Aviva Levina, Peter Turner, and Peter A. Lay*

Centre for Heavy Metals Research, School of Chemistry, University of Sydney, Sydney, NSW 2006, Australia

Received January 16, 2003

X-ray absorption spectroscopy (XAS) provides a direct means of solving the controversy on Cr oxidation states in nitroso complexes. The first XAS studies of four known Cr–NO complexes, $[Cr(NO)(OH_2)_5]^{2+}$, $[Cr(NO)(acac)_2(OH_2)]$, $[Cr(NO)(CN)_5]^{3-}$, and $[Cr(NO)(NCS)_5]^{3-}$, have been performed, in comparison with the related Cr(III) complexes, $[Cr(OH_2)_6]^{3+}$, $[Cr(acac)_3]$, $[Cr(CN)_6]^{3-}$, and $[Cr(NCS)_6]^{3-}$. The X-ray absorption near-edge structure (XANES) spectra of the Cr–NO complexes are distinguished from those of the corresponding Cr(III) complexes by increased intensities of pre-edge absorbancies due to the 1s → 3d transition, as well as with slight shifts (by 0.2–1.0 eV) of the edge positions to lower energies, with no major changes in the edge shape. These features, together with the available structural data on Cr–NO complexes, show that the effective Cr oxidation states in such complexes are close to Cr(III), due to the π-back-bonding within the Cr–NO moiety. Multiple-scattering fitting of X-ray absorption fine structure (XAFS) spectra of $[Cr(NO)(acac)_2(OH_2)]$ supported the assignment of this complex as a *trans*-isomer (Keller, A.; Ježovska-Trzebiatowska, B. *Polyhedron* **1985**, *4*, 1847–1852). The first crystal structure of a Cr nitroso–isothiocyanato complex, $(Ph_4P)_3[Cr(NO)(NCS)_5]\cdot 2.4(CH_3)_2CO$, has been determined.

Introduction

The chemistry of metal nitrosyl complexes is an area of current interest due to the diverse physiological roles ascribed to NO complexes with metalloenzymes.[1] Chromium nitrosyl complexes, due to their relative chemical stability and kinetic inertness, are used as models for understanding the nature of bonding and chemical properties of metal nitrosyls.[2] There has been much debate in the literature on the assignment of Cr oxidation states in such complexes ($Cr^{I}-NO^{+}$, $Cr^{II}-NO^{\bullet}$, or $Cr^{III}-NO^{-}$).[2,3] The first assignment (Cr(I), d^5 species) is based on the sharp intense signals in electron paramagnetic resonance (EPR) spectra at room temperature, typical magnetic susceptibilities of 1.8−2.0 μ_B, and the IR-spectroscopic evidence for the presence of NO^+ group.[4−10] The structure of a Cr nitroso−aqua complex (determined by X-ray crystallography) has been interpreted as being close to $[Cr^{III}(NO^-)(OH_2)_5]^{2+}$,[2] in agreement with the kinetic inertness and stability toward oxidation, characteristic for this compound.[2,11] On the other hand, density functional theory (DFT) calculations for this complex led to the values of the Cr oxidation states close to Cr(II) (from +1.65 to +1.84).[12] Measurements of the core-electron binding energies by X-ray photoelectron spectroscopy (XPS) led to close values for $[Cr(NO)(CN)_5]^{3-}$ and $[Cr(CN)_6]^{3-}$, leading to the assignment of the former complex as a Cr(III) species.[13]

* To whom correspondence should be addressed. E-mail: p.lay@chem.usyd.edu.au.

(1) (a) Hayton, T. W.; Legzdins, P.; Sharp, W. B. *Chem. Rev.* **2002**, *102*, 935−991. (b) Ford, P. C.; Lorkovic, I. M. *Chem. Rev.* **2002**, *102*, 993−1017 and references therein.
(2) Ardon, M.; Cohen, S. *Inorg. Chem.* **1993**, *32*, 3241−3243.
(3) Larkworthy, L. F.; Nolan, K. B.; O'Brien, P. In *Comprehensive Coordination Chemistry*; Wilkinson, G., Gillard, R. D., McCleverty, J. A., Eds.; Pergamon Press: Oxford, U.K., 1987; Vol. 3, pp 699−969 and references therein.
(4) Griffith, W. P.; Lewis, J.; Wilkinson, G. *J. Chem. Soc.* **1959**, 872−875.
(5) Ardon, M.; Herman, J. I. *J. Chem. Soc.* **1962**, 507−509.
(6) Griffith, W. P. *J. Chem. Soc.* **1963**, 3286−3291.
(7) Meriwether, L. S.; Robinson, S. D.; Wilkinson, G. *J. Chem. Soc. A* **1966**, 1488−1491.
(8) Manoharan, P. T.; Gray, H. B. *Inorg. Chem.* **1966**, *5*, 823−839.
(9) Rieger, P. H. *Coord. Chem. Rev.* **1994**, *135/136*, 203−286.
(10) Carruthers, L. M.; Closken, C. L.; Link, K. L.; Mahapatro, S. N.; Bikram, M.; Du, J.-L.; Eaton, S. S.; Eaton, G. R. *Inorg. Chem.* **1999**, *38*, 3529−3534.
(11) Jhanji, A. K.; Gould, E. S. *Inorg. Chem.* **1990**, *29*, 3890−3892.
(12) Shim, I.; Gingerich, K. A.; Mandix, K.; Feng, X. *Inorg. Chim. Acta* **1995**, *229*, 455−460.

10.1021/ic0340480 CCC: $25.00
Published on Web 07/23/2003

X-ray absorption spectroscopy (XAS) provides a direct means of measurement of metal oxidation states in coordination compounds, by comparison of the pre-edge and edge (X-ray absorption near-edge structure, XANES) features of the spectra with those of model complexes.[14−18] In this work, the first XAS study of Cr−NO complexes has been performed, using well-characterized Cr(III) complexes as reference compounds.

Experimental Section

Reagents and Syntheses. The following commercially available compounds of analytical or higher purity grades were used without further purification: acetone (HPLC grade), acetylacetone, thiourea, CrO_3, $NH_2OH{\cdot}HCl$, $(Ph_4P)Cl$, $K_3[Cr(CN)_6]$ (99.9%), and BN from Aldrich; K_2CrO_4, $Cr(NO)_3{\cdot}9H_2O$ ($[Cr(OH_2)_6](NO_3)_3{\cdot}3H_2O$),[19] H_2SO_4, KOH, KCN, KSCN, $(NH_4)SCN$, Na_2CO_3, and $NaHCO_3$ from Merck; and Dowex 50 ×2 cation-exchange resin (100−200 mesh) from Fluka. The following complexes were synthesized by literature methods: $[Cr(NO)(acac)_2(OH_2)]$ [acac = acetylacetonato(1−) = 2,4-pentadionato(1−)],[20] $K_3[Cr(NO)(CN)_5]{\cdot}H_2O$,[4] $(Ph_4P)_3[Cr(NO)(NCS)_5]$,[21] $[Cr(acac)_3]$,[22] and $K_3[Cr(NCS)_6]{\cdot}4H_2O$.[23] The results of elemental analyses, magnetic susceptibility measurements, and EPR, ultraviolet−visible (UV−vis), and infrared (IR) spectroscopies for all the synthesized complexes (Table 1 and Figures S1−S3 in Supporting Information) were consistent with the literature data.[3−10,20−23] Recrystallization of crude $(Ph_4P)_3[Cr(NO)(NCS)_5]$ from acetone yielded relatively small (0.2−0.3 mm) crystals of a solvated complex, suitable for X-ray crystallography. Attempts to grow larger crystals from various solvents were unsuccessful as yet, since prolonged storage of the complex in solutions led to the loss of NO and the formation of $[Cr(NCS)_6]^{3-}$ (as shown by UV−vis spectroscopy, Figure S2).

The $[Cr(NO)(OH_2)_5]^{2+}$ complex was generated in aqueous solutions by the reaction of CrO_3 with $NH_2OH{\cdot}HCl$ and purified by ion-exchange chromatography, as described previously.[2,10] The UV−vis spectra of the purified solutions corresponded to the literature data for $[Cr(NO)(OH_2)]^{2+}$ (Figure S2, Cr concentration, 35−40 mM).[2] However, repeated attempts to obtain crystalline $[Cr(NO)(OH_2)_5](SO_4)$ by slow evaporation of the aqueous solutions after chromatography (containing ∼0.5 M H_2SO_4 used as eluent)[2] were unsuccessful. In acidic solution, the nitroso complex hydrolyzed to $[Cr(OH_2)_6]^{3+}$ (as evident from UV−vis spectroscopy, Figure S2, and from the color change from brown to blue) within ∼7 days at ambient conditions. When the pH value of the solution was maintained at 2.0 ± 0.5 during the evaporation (by additions of solid $NaHCO_3$), a mixture of $[Cr(NO)(OH_2)_5](SO_4)$ and Na_2SO_4 (brown solid; Cr content, ∼4% mass) was formed after ∼14 days; this mixture was used for the XAS experiments.

Table 1. Crystallographic Data for $(Ph_4P)_3[Cr(NO)(NCS)_5]{\cdot}2.4(CH_3)_2CO$

formula of the refinement model	$C_{84.20}H_{74.40}CrN_6O_{3.40}P_3S_5$
model molecular wt	1529.91
cryst syst	triclinic
space group	$P\bar{1}$ (No. 2)
a	13.401(6) Å
b	17.707(7) Å
c	18.773(8) Å
α	77.902(7)°
β	78.326(7)°
γ	71.572(7)°
V	4088(3) Å^3
D_c	1.243 g cm^{-3}
Z	2
cryst size	0.340 × 0.220 × 0.130 mm^3
cryst color	brown
cryst habit	tablet
temp	150(2) K
λ(Mo Kα)	0.71073 Å
μ(Mo Kα)	0.377 mm^{-1}
T(Gaussian)$_{min,max}$	0.865, 0.958
$2\theta_{max}$	56.62°
hkl range	−17 17, −22 23, −24 24
N	41171
N_{ind}	19242(R_{merge}0.0398)
N_{obs}	12196 ($I > 2\sigma(I)$)
N_{var}	900
residuals[a] R1(F), wR2(F^2)	0.0504, 0.1241
GOF (all)	1.357
residual extrema	−0.724, 0.848 e$^-$ Å^{-3}

[a] $R1 = \sum||F_o| - |F_c||/\sum|F_o|$ for $F_o > 2\sigma(F_o)$; $wR2 = (\sum w(F_o^2 - F_c^2)^2/\sum(wF_c^2)^2)^{1/2}$; all reflections $w = 1/[\sigma^2(F_o^2) + (0.03P)^2 + 0.8P]$, where $P = (F_o^2 + 2F_c^2)/3$.

Analytical Techniques. Determinations of Cr in the solid samples (after their digestion with 69% HNO_3; Table S1) were performed using a Varian SpectrAA-800 atomic absorption spectrometer with C_2H_2−air flame atomization, calibrated with Cr(III) standards (Aldrich). Elemental analyses (C, H, N, S; Table S1) were performed by the Australian National University Microanalytical Unit, using a Carlo Erba 1106 automatic analyzer. Magnetic susceptibility (Table S1) was measured on a Sherwood Scientific magnetic susceptibility balance. The balance was calibrated with $(NH_4)_2Fe(SO_4)_2{\cdot}6H_2O$, and diamagnetic corrections for the constituent atoms were calculated from the literature.[24] Solution EPR spectra (X-band, Figure S1) were acquired on a Bruker EMX spectrometer, using Wilmad quartz flat cell; calibrations of the magnetic field and the microwave frequency were performed with an EMX 035 NMR gaussmeter and an EMX 048T microwave bridge controller, respectively. The instrumental settings were as follows: center field, 3460−3500 G; sweep width, 200 G (Cr−NO complexes) or 1000 G (Cr(III) complexes); resolution, 1024 points; microwave power, 2.0 mW; microwave frequency, ∼9.67 GHz; modulation frequency, 100 kHz; modulation amplitude, 0.40 G (Cr−NO complexes) or 5.0 G (Cr(III) complexes); time constant, 20.48 ms; receiver gain, 10^3−10^4; and number of scans, 5. The EPR spectral parameters (Table S1) were determined by simulation of the spectra with

(13) Hendrickson, D. N.; Hollander, J. M.; Jolly, W. L. *Inorg. Chem.* **1970**, *9*, 612−615.
(14) Sutton, S. R.; Jones, K. W.; Gordon, B.; Rivers, M. L.; Bajt, S.; Smith, J. V. *Geochim. Cosmochim. Acta* **1993**, *57*, 461−468.
(15) (a) Berry, A. J.; Shelley, J. M. G.; Foran, G. J.; O'Neill, H. S. C.; Scott, D. R. *J. Synchrotron Radiat.* **2003**, *10*, 332−336. (b) Berry, A. J.; O'Neill, H. S. C. To be submitted.
(16) Ellis, P. J.; Joyner, R. W.; Maschmeyer, T.; Masters, A. F.; Niles, D. A.; Smith, A. K. *J. Mol. Catal. A: Chem.* **1996**, *111*, 297−305.
(17) Dillon, C. T.; Lay, P. A.; Cholewa, M.; Legge, G. J. F.; Bonin, A. M.; Collins, T. J.; Kostka, K. L.; Shea-McCarthy, G. *Chem. Res. Toxicol.* **1997**, *10*, 533−535.
(18) Pattison, D. I.; Levina, A.; Davies, M. J.; Lay, P. A. *Inorg. Chem.* **2001**, *40*, 214−217.
(19) Lazar, D.; Ribár, B.; Divjaković, V.; Mészáros, C. *Acta Crystallogr., Sect. C* **1991**, *C47*, 1060−1062.
(20) Keller, A.; Ježowska-Trzebiatowska, B. *Polyhedron* **1985**, *4*, 1847−1852.
(21) Bhattacharyya, R. G.; Bhattacharjee, G. P.; Roy, P. S. *Inorg. Chim. Acta* **1981**, L263−L264.
(22) *Handbook of Preparative Inorganic Chemistry*, 2nd ed.; Brauer, G., Ed.; Academic Press: New York, 1965; Vol. 2, pp 1383−1384.
(23) *Handbook of Preparative Inorganic Chemistry*, 2nd ed.; Brauer, G., Ed.; Academic Press: New York, 1965; Vol. 2, pp 1374−1375.
(24) Mabbs, F. E.; Machin, D. J. *Magnetism and Transition Metal Complexes*; Chapman and Hall: London, 1973.

WinSim;[25] second-order corrections were applied in the simulations. A Hewlett-Packard HP 8452A diode-array spectrophotometer was used for UV−vis spectroscopic measurements (Figure S2). Solid-state IR spectra (Figure S3) were recorded using a diffuse reflectance technique (for the mixtures with KBr) on a BioRad FTS-40 spectrometer. All the spectroscopic and magnetic measurements were performed at room temperature (295 ± 1 K).

X-ray Absorption Spectroscopy and Data Processing. Chromium K-edge spectra of the Cr−NO and Cr(III) complexes were recorded on the Australian National Beamline Facility (beamline 20B) at the Photon Factory, Tsukuba, Japan. The beam energy was 2.5 GeV, and the beam current, 300−400 mA. A Si[111] double-crystal monochromator was detuned by 50%. Solid samples were mixed with BN (0.5−2 mass parts per 1 part of a Cr complex) and pressed into 0.5-mm pellets supported in an Al spacer between two 63.5-μm Kapton tape windows. Room temperature (295 K) spectra were recorded in transmission mode, using N_2/He-filled ionization chambers. Low-temperature XAS spectra (17 ± 1 K; maintained with a closed-cycle He CryoIndustries REF-1577-D22 cryostat) were collected for some of the complexes (see Results section) using fluorescence detection mode (10-element Ge-array detector). Collection of XAS data at low temperature minimized sample photodamage, improved the signal-to-noise ratio, and maximized the (multiple-scattering) MS contributions to the (X-ray absorption fine structure) XAFS spectrum.[26] The spectra were averaged from three scans taken at different positions on the sample; no color changes at irradiated spots were observed, and the edge energies differed by <0.1 eV between the scans. The following energy ranges were used for the data collection: pre-edge region, 5770−5970 eV (10 eV steps); XANES region, 5970−6050 eV (0.25 eV steps); and XAFS region, 6050−7000 eV (0.05 Å^{-1} steps in *k*-space). The energy scale was calibrated using a Cr foil as an internal standard (calibration energy, 5989.0 eV, corresponded to the first peak of the first derivative of Cr(0) edge).[27] Averaging, background subtraction, and the calculations of theoretical XAFS spectra (using MS models) were performed using the *XFIT* software package,[27] including *FEFF 6.01*[28] algorithm, as described previously.[26] Conditions, restraints, and constraints applied to the calculations are listed in Supporting Information. The determinancies (N_i/p, where N_i is the number of independent observations and p is the number of varied parameters) of the models used in SS and MS XAFS calculations were estimated by the method of Binsted et al.,[29] taking into account the applied restraints and constraints. Overdetermined models ($N_i/p > 1$) were used in XAFS calculations, which allowed meaningful solutions to be obtained.[29] In the MS XAFS calculations, the values of bond lengths and bond angles within the acac ligands (for $[Cr(NO)(acac)_2(OH_2)]$) were restrained to be close (±0.02 Å; ±2°) to those found in the crystal structure of $[Cr(acac)_3]$.[30] Release of these restraints led to underdetermined ($N_i/p < 1$) fits and to implausible distortions in the ligand structures. Debye−Waller factors of similar atoms in the ligands were constrained to be equal, thereby decreasing the number of variables in the models. Typically, convergence in MS XAFS calculations was achieved after 200−300 iterations. The random errors in the estimated XAFS parameters, arising from the noise in the data, were determined by Monte Carlo analysis within the *XFIT* software.[27] Starting coordinate sets for different models, used for MS XAFS calculations, were obtained using *HyperChem* software.[31]

X-ray Crystallography. Crystallographic data for $(Ph_4P)_3[Cr(NO)(NCS)_5]\cdot 2.4(CH_3)_2CO$ are summarized in Table 1. A brown tablet-like crystal was attached with Exxon Paratone N, to a short length of fiber supported on a thin piece of copper wire inserted in a copper mounting pin. The crystal was quenched in a cold nitrogen gas stream from an Oxford Cryosystems Cryostream. A Bruker SMART 1000 CCD diffractometer employing graphite monochromated Mo Kα radiation generated from a sealed tube was used for the data collection. Cell constants were obtained from a least-squares refinement against 1008 reflections located between 5° and 53° 2θ. Data were collected at 150 ± 2 K with ω scans to 56.62° 2θ. The data integration and reduction were undertaken with *SAINT* and *XPREP*,[32] and subsequent computations were carried out with the *teXsan*,[33] *WinGX*,[34] and *XTAL*[35] graphical user interfaces. The intensities of 171 standard reflections re-collected at the end of the experiment did not change significantly during the data collection. A Gaussian absorption correction[36] was applied to the data.

The structure was solved in the space group $P\bar{1}$ (No. 2) by direct methods with *SIR97*,[37] and extended and refined with *SHELXL-97*.[38] The asymmetric unit contains the $[Cr(NO)(NCS)_5]^{3-}$ complex molecule, three Ph_4P^+ counterions, and two acetone solvate molecules disordered about two slightly different orientations. There is additionally a third acetone site, with an occupancy refined and then fixed at 0.4. The cationic nitrosyl ligand is site disordered over the six octahedral coordination sites, with occupancies of 0.8, 0.02, 0.08, 0.05, 0.03, and 0.02 obtained by refinement of the complementary isothiocyanate sulfur site populations. The low occupancy nitrosyl ligand sites were modeled with restraints and rigid groups. The disordered acetone molecules were modeled with rigid bodies. In general, the non-hydrogen atom sites were modeled with anisotropic displacement parameters, and a riding atom model was used for the hydrogen atoms. The non-hydrogen atom sites with occupancies of less than 0.9 were modeled with isotropic displacement parameters.

Results

XANES Spectra. The edge shapes for Cr−NO complexes were similar to those of the corresponding Cr(III) complexes (Figures 1 and S4). All the studied Cr−NO complexes were distinguished from the corresponding Cr(III) complexes by increased pre-edge absorbances due to a symmetry-forbidden 1s → 3d transition[14−18] (A in Figure 1 and Table 2), and by

(25) Duling, D. R. *J. Magn. Reson.* **1994**, *B104*, 105−110. The software is available via the Internet at http://epr.niehs.nih.gov/.

(26) (a) Rich, A. M.; Armstrong, R. S.; Ellis, P. J.; Freeman, H. C.; Lay, P. A. *Inorg. Chem.* **1998**, *37*, 5743−5753. (b) Rich, A. M.; Armstrong, R. S.; Ellis, P. J.; Lay, P. A. *J. Am. Chem. Soc.* **1998**, *120*, 10827−10836.

(27) (a) Ellis, P. J.; Freeman, H. C. *J. Synchrotron Radiat.* **1995**, *2*, 190−195. (b) *XFIT for Windows'95*; Australian Synchrotron Research Program: Sydney, Australia, 1996.

(28) Rehr, J. J.; Albers, R. C.; Zabinsky, S. I. *Phys. Rev. Lett.* **1992**, *69*, 3397−3400.

(29) Binsted, N.; Strange, R. W.; Hasnain, S. S. *Biochemistry* **1992**, *31*, 12117−12125.

(30) Morosin, B. *Acta Crystallogr.* **1965**, *19*, 131−137.

(31) *HyperChem*, version 5.1; Hypercube Inc.: Gainesville, FL, 1996.

(32) *SMART, SAINT and XPREP. Area detector control and data integration and reduction software*; Bruker Analytical X-ray Instruments Inc.: Madison, WI, 1995.

(33) *teXsan for Windows: Single Crystal Structure Analysis Software*; Molecular Structure Corporation: The Woodlands, TX, 1997.

(34) Farrugia, L. J. *J. Appl. Crystallogr.* **1999**, *32*, 837−838.

(35) *Xtal3.6 System*; Hall, S. R., du Boulay, D. J., Olthof-Hazekamp, R., Eds.; University of Western Australia: Perth, Australia, 1999.

(36) Coppens, P.; Leiserowitz, L.; Rabinovich, D. *Acta Crystallogr.* **1965**, *18*, 1035−1038.

(37) Altomare, A.; Burla, M. C.; Camalli, M.; Cascarano, G. L.; Giacovazzo, C.; Guagliardi, A.; Moliterni, A. G. G.; Polidori, G.; Spagna, R. *J. Appl. Crystallogr.* **1998**, *32*, 115−119.

(38) Sheldrick, G. M. *SHELX97 Programs for Crystal Structure Analysis*; University of Göttingen: Göttingen, Germany, 1998.

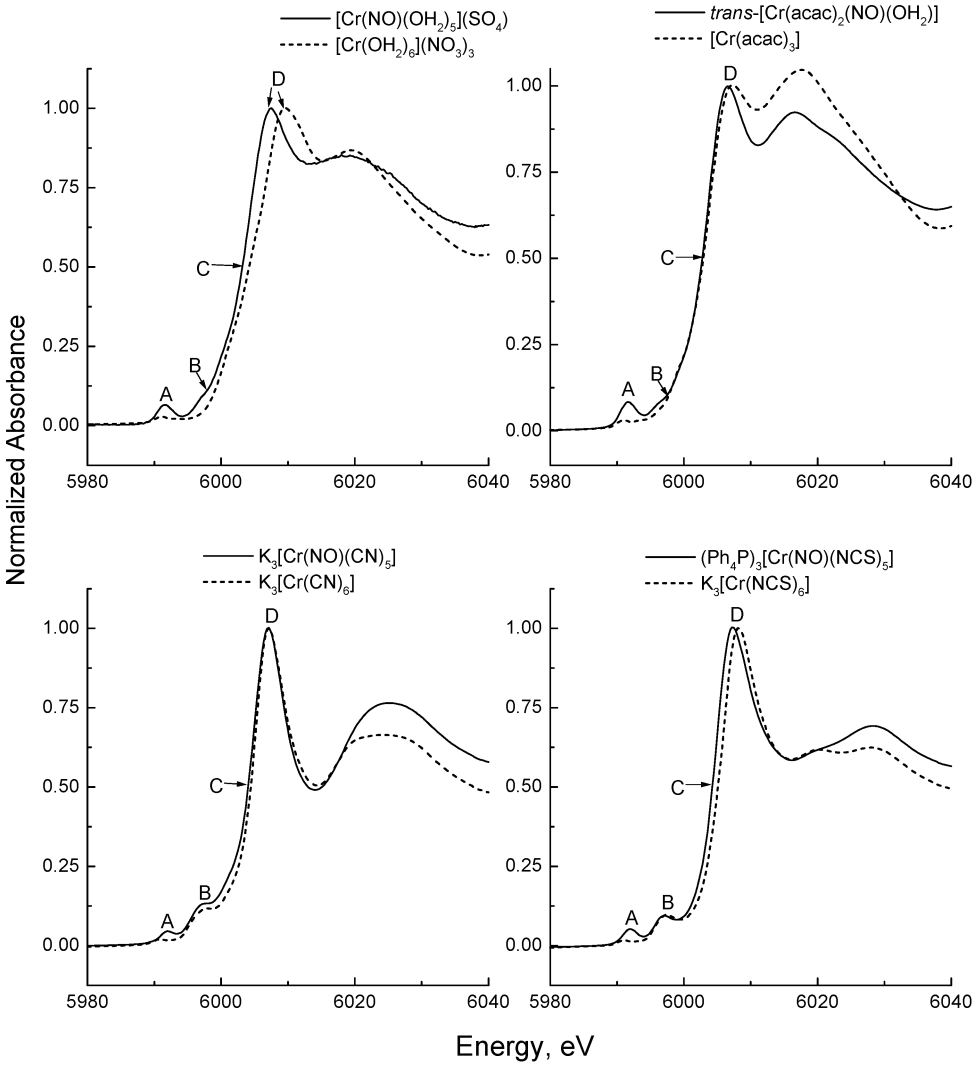

Figure 1. Comparison of XANES spectra of the Cr−NO and Cr(III) complexes. All spectra were taken at 295 K (transmission mode), except for that of $[Cr(NO)(OH_2)_5](SO_4)$ (17 K, fluorescence mode). Designations of the XANES features (A−D) correspond to Table 2.

Table 2. Parameters of XANES Spectra of the Cr−NO Complexes and the Related Cr(III) Complexes

		XANES features,[a] eV			
complex	*T*, K	A[b]	B	C	D
$[Cr(NO)(OH_2)_5]^{2+}$	17	5991.6 (6.3)	5998.1	6003.1	6007.5
$[Cr(OH_2)_6]^{3+}$	295	5991.1 (2.8)		6004.2	6009.6
trans-$[Cr(NO)(acac)_2(OH_2)]$	295	5991.7 (8.1)	5997.3	6002.7	6006.5
$[Cr(acac)_3]$	295	5991.0 (3.0)		6002.9	6007.4
$[Cr(NO)(CN)_5]^{3-}$	17	5991.8 (4.2)	5997.6	6004.0	6007.1
$[Cr(NO)(CN)_5]^{3-}$	295	5991.9 (4.7)	5997.8	6004.0	6007.0
$[Cr(CN)_6]^{3-}$	17	5991.0 (2.4)	5998.3	6004.5	6007.0
$[Cr(CN)_6]^{3-}$	295	5990.9 (2.1)	5997.7	6004.4	6007.2
$[Cr(NO)(NCS)_5]^{3-}$	295	5992.0 (5.2)	5997.1	6004.2	6007.3
$[Cr(NCS)_6]^{3-}$	295	5991.1 (1.6)	5997.4	6005.1	6008.2

[a] A and B are the pre-edge absorbances, C corresponds to 50% of the edge jump, and D is the edge crest (Figures 1 and S4). [b] Absorbance intensities (in % of the normalized edge jump) are given in parentheses.

slight shifts (0.2−1.0 eV) of the edge positions to lower energies (C and D in Figure 1 and Table 2). In addition, shoulders at ∼5997 eV (∼8% of the edge jump) appeared in the XANES spectra of $[Cr(NO)(OH_2)_5](SO_4)$ and $[Cr(NO)(acac)_2(OH_2)]$, but not in those of the corresponding Cr(III) complexes (B in Figure 1 and Table 2). There were no qualitative differences in the XANES spectra taken at 295 K or at 17 K (for $K_3[Cr(NO)(CN)_5]$ and $K_3[Cr(CN)_6]$, Figure 1 and Figure S4 in Supporting Information).

XAFS Spectra. Detailed analyses of XAFS spectra were performed for two of the studied complexes: (i) $[Cr(NO)(OH_2)_5](SO_4)$, which was not isolated as a pure solid in this work; and (ii) $[Cr(NO)(acac)_2(OH_2)]$, which has not yet been characterized by X-ray crystallography. Experimental spectra and MS XAFS fits for these complexes are shown in Figures 2 and 3, the optimized values of the Cr−ligand bond lengths and the Cr−N−O angles are listed in Table 3, the optimized structures of the complexes are shown in Figure 4 and Figure S5 (Supporting Information), and details of the conditions and results of MS XAFS analyses are given in Tables S2−S7, Supporting Information.

An excellent fit ($R = 11.9\%$, Figure 2) was obtained for $[Cr(NO)(OH_2)_5](SO_4)$, and the optimized structural parameters (Tables 3 and S3 and Figure S5) agreed with those found in the crystal structure (within 0.02 Å or 2°, which are the usual "conservative estimates" for systematic errors in MS XAFS calculations),[26] except for a slightly shorter Cr−O bond *trans* to the NO group (2.01 vs 2.05 Å in the crystal structure). For the $[Cr(NO)(acac)_2(OH_2)]$ complex,

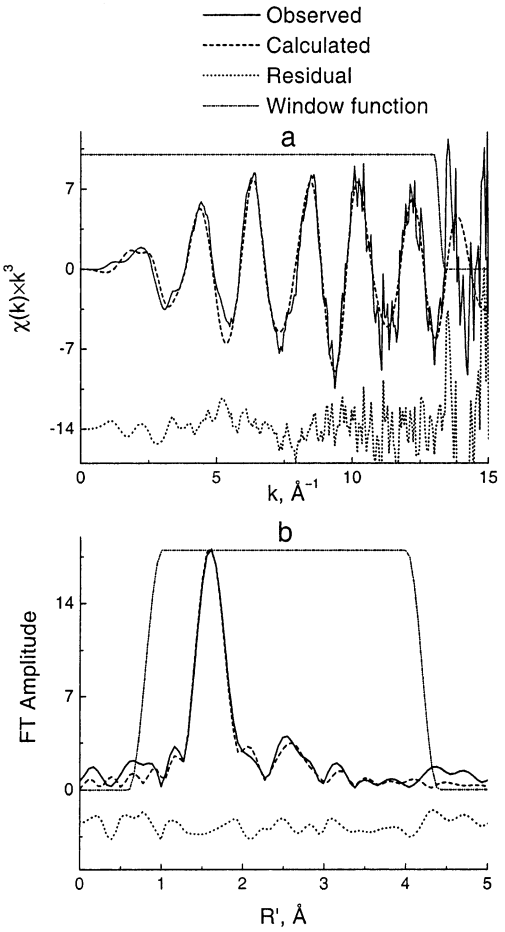

Figure 2. Experimental and calculated (MS fits) XAFS (a) and Fourier transform (FT) XAFS (b) spectra for $[Cr(NO)(OH_2)_5](SO_4)$ (solid mixture with Na_2SO_4, 17 K, fluorescence mode). Optimized structure of the complex is shown in Figure S5, and details of the XAFS calculations are given in Tables S2−S4, Supporting Information.

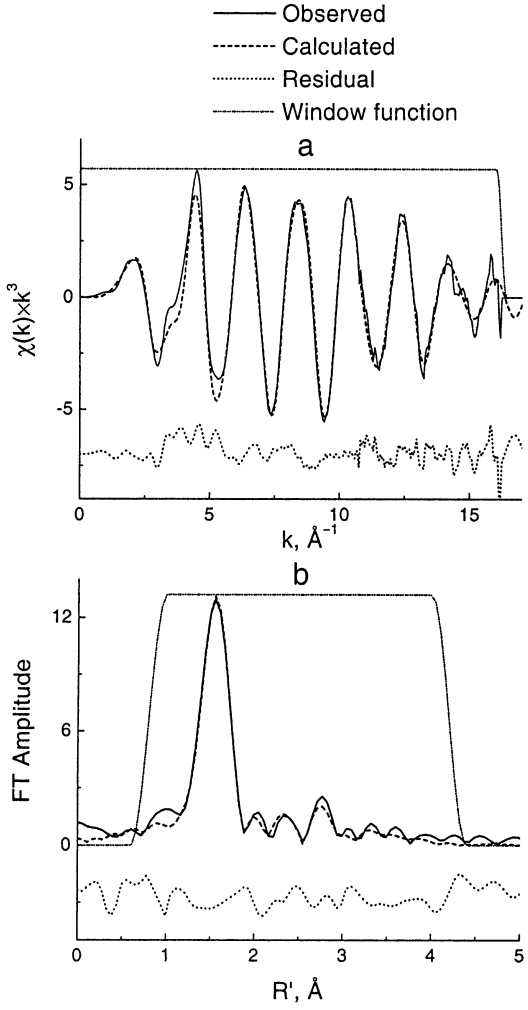

Figure 3. Experimental and calculated (MS fits) XAFS (a) and FT XAFS (b) spectra for $[Cr(NO)(acac)_2(OH_2)]$ (solid mixture with BN, 295 K, transmission mode). Details of the XAFS calculations are given in Tables S5−S7, Supporting Information.

two independent models with the NO and aqua ligands in *trans*- or *cis*-positions were used for MS XAFS calculations; the former model resulted in a significantly better fit (R = 11.4 vs 13.2%, Figure 3 and Table S6). Structural parameters of the optimized *trans*-$[Cr(NO)(acac)_2(OH_2)]$ model (Figure 4), including a short Cr−N bond, an elongated axial Cr−O bond, and a nearly linear Cr−N−O angle, were consistent with the crystallographic data for the $[Cr(NO)(OH_2)_5]^{2+}$ complex and related Cr−NO compounds (Table 3).[2,39,40] The Cr−O bonds for the acac ligands (1.96 ± 0.02 Å, Table 3) were within experimental error of the average value for the $[Cr(acac)_3]$ complex (1.951 Å).[30]

X-ray Crystal Structure of $(Ph_4P)_3[Cr(NO)(NCS)_5]\cdot 2.4(CH_3)_2CO$. An ORTEP[41] depiction of the $[Cr(NO)(NCS)_5]^{3-}$ anion (with 50% displacement ellipsoids), showing the disorder of the NO ligand (see Experimental Section), is given in Figure 5, selected structural data are listed in Table 3, and detailed results of X-ray crystallography are available as a CIF file. The structure shows the common features of Cr−NO complexes, as already mentioned. The Cr−N(NCS) bonds in $[Cr(NO)(NCS)_5]^{3-}$ (2.01−2.07 Å, Table 3) were significantly longer than the corresponding values in $[Cr(NCS)_6]^{3-}$ (1.94−2.00 Å, dependent on the nature of the counterion).[3,42,43]

Discussion

The results of MS fitting of XAFS spectra for $[Cr(NO)(OH_2)_5](SO_4)$ and $[Cr(NO)(acac)_2(OH_2)]$ (Figures 2−4 and Table 3) confirmed the integrity of microcrystalline Cr−NO compounds, used in this work (a solid mixture with Na_2SO_4 for the former complex and a pure microcrystalline powder for the latter). In addition, these results support the assignment of the $[Cr(NO)(acac)_2(OH_2)]$ complex as a *trans*-isomer, made on the basis of EPR- and IR-spectroscopic data.[20] The slightly shorter axial Cr−O(OH_2) bond length in $[Cr(NO)(OH_2)_5]^{2+}$, determined by MS XAFS calculations, compared with that found in the crystal structure (2.01 vs

(39) Enemark, J. H.; Quinby, M. S.; Reed, L. L.; Steuck, M. J.; Walthers, K. K. *Inorg. Chem.* **1970**, *9*, 2397−2403.
(40) Shibahara, T.; Akashi, H.; Asano, M.; Wakamatsu, K.; Nishimoto, K.; Mori, M. *Inorg. Chem. Commun.* **2001**, *4*, 413−415.
(41) Johnson, C. K. *ORTEPII*; Report ORNL-5138; Oak Ridge National Laboratory: Oak Ridge, TN, 1976.
(42) Cherkasova, T. G. *Zh. Neorg. Khim.* **1994**, *39*, 1316−1319; *Russ. J. Inorg. Chem. (Engl. Trans.)* **1994**, *39*, 1255−1258.
(43) Enemark, J. H.; Feltham, R. D. *J. Am. Chem. Soc.* **1974**, *96*, 5002−5004.

Table 3. Selected Bond Lengths and Angles in Cr−NO Complexes

complex	method[a]	Cr−N(NO), Å	Cr−lig,[b] Å	Cr−lig,[c] Å	N−O, Å	Cr−N−O, deg	ref
$[Cr(NO)(OH_2)_5]^{2+}$	XRD	1.682(2)	2.057(2)	1.986(2)	1.186(3)	177.0(2)	2
$[Cr(NO)(OH_2)_5]^{2+}$	XAFS	1.69(2)	2.01(2)	1.98(2)	1.18(2)	177(2)	this work
trans-$[Cr(NO)(acac)_2(OH_2)]$	XAFS	1.69(2)	2.05(2)	1.96(2)	1.17(2)	176(2)	this work
$[Cr(NO)(CN)_5]^{3-}$	XRD	1.71(1)	2.07(1)	2.033(7)	1.21(1)	176(1)	39
$[Cr(NO)(NH_3)_5]^{2+}$	XRD	1.677(6)	2.140(5)	2.096(4)	1.180(7)	179.9(6)	40
$[Cr(NO)(NCS)_5]^{3-}$ [d]	XRD	1.708(2)	2.069(2)	2.014(2)	1.187(1)	177.1(3)	this work

[a] XRD = X-ray diffraction on a single crystal. [b] For the ligands in axial position in relation to the NO group. [c] For the ligands in equatorial position in relation to the NO group. [d] The results for the most populated site (80% occupancy, see Experimental Section).

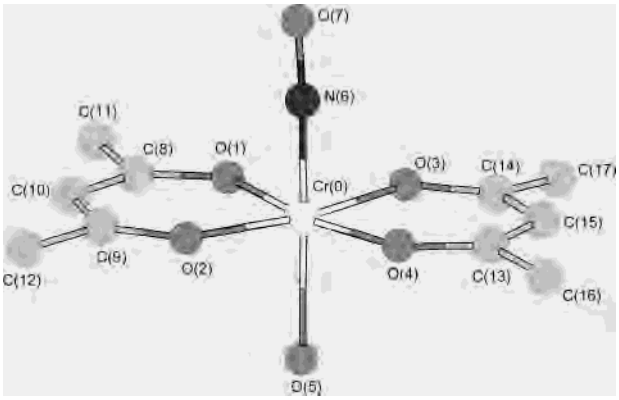

Figure 4. Structure of *trans*-$[Cr(NO)(acac)_2(OH_2)]$ (295 K), optimized by MS fitting of XAFS data.

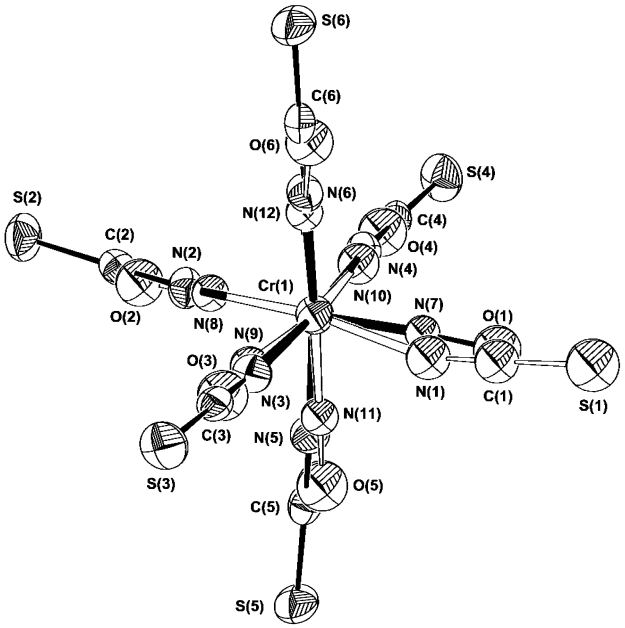

Figure 5. ORTEP depiction (with 50% displacement ellipsoids) of $[Cr(NO)(NCS)_5]^{3-}$, showing the disorder of the nitrosyl ligand.

2.05 Å, Table 3),[2] may point to the presence of deprotonated species (*trans*-$[Cr(NO)(OH)(OH_2)_4]^{+}$) in the bulk material, or crystal packing forces.

Although the linear Cr−N−O units in the studied Cr−NO complexes (Table 3) are consistent with a formal oxidation state of Cr(I) with a NO^+ ligand,[1] the results of XAS rule out the assignment of the effective oxidation states of the metal as Cr(I),[4−10] or Cr(II).[12] Reduction of Cr(III) to Cr(II) in octahedral complexes with O-donor ligands causes edge shifts to lower energies by ∼5 eV (as measured at the edge crest, D in Figure 1),[15] as well as the appearance of a shoulder at ∼50% of the edge jump, attributed to a 1s → 4s transition.[14−16] Both these diagnostic features of Cr(II) are not observed in the Cr−NO complexes (Figure 1 and Table 2). Although no XAS data for nonorganometallic Cr(I) complexes are available as yet, the difference in edge energies between Cr(I) and Cr(III) complexes is expected to be even higher that that for Cr(II) and Cr(III) complexes.[14−18]

Comparison of the edge energies of Cr−NO complexes with those of the related Cr(III) compounds (C and D in Figure 1 and Table 2) shows that the effective oxidation states of Cr in the former complexes are only slightly lower than Cr(III). Indeed, the differences in the edge energies in the pairs of related Cr−NO and Cr(III) complexes (up to 1.0 eV) are smaller than such differences between Cr(III) complexes with different ligands (up to 2.2 eV, Table 2). This finding, which is consistent with the earlier results of XPS spectroscopy,[13] and kinetic studies,[11] is explained by the formation of a Cr≡NO triple bond by overlapping between two π^* orbitals of NO and two dπ orbitals of Cr (π-back-bonding), leading to the short (1.69−1.70 Å) Cr−NO distances.[1,12,40] The XANES spectroscopic data (Figure 1 and Table 2) are consistent with the results of molecular orbital calculations for $[Cr(NO)(CN)_5]^{3-}$ and $[Cr(NO)(acac)_2(OH_2)]$ (Figure 6).[8,20] The apparent d^5 electronic state of the metal ion in Cr−NO complexes (reflected in the EPR spectra and magnetic susceptibilities)[5−10,20] is caused by the covalent interactions within the Cr−NO moiety (Figure 6).[1,43] Similarly, analysis of XANES data for Cr−CO complexes (formally Cr(0) species) pointed to effective oxidation states of Cr between Cr(III) and Cr(IV) due to extensive π-back-bonding (Cr metal, Cr_2O_3, and CrO_2 were used as the reference compounds).[44]

Distortions in the octahedral structures of Cr−NO complexes due to the short Cr−NO bonds are reflected in the increased pre-edge absorbance features in XANES spectra,[16−18] compared with the corresponding Cr(III) complexes (A in Figure 1 and Table 2). The appearance of a new pre-edge absorbance band (B in Figure 1 and Table 2; ∼8% of the normalized edge jump) in the XANES spectra of $[Cr(NO)(OH_2)_5](SO_4)$ and $[Cr(NO)(acac)_2(OH_2)]$ (compared with the corresponding Cr(III) complexes) can be attributed to mixing of p- and d-orbitals due the π-bonding and back-bonding (Figure 6). This assignment is supported by the presence of band B in the XANES spectra of Cr(III) complexes with π-acid/base ligands, $K_3[Cr(CN)_6]$ and $K_3[Cr(NCS)_6]$ (Figure

(44) Engemann, C.; Hormes, J.; Longen, A.; Dötz, K. H. *Chem. Phys.* **1998**, *237*, 471−481.

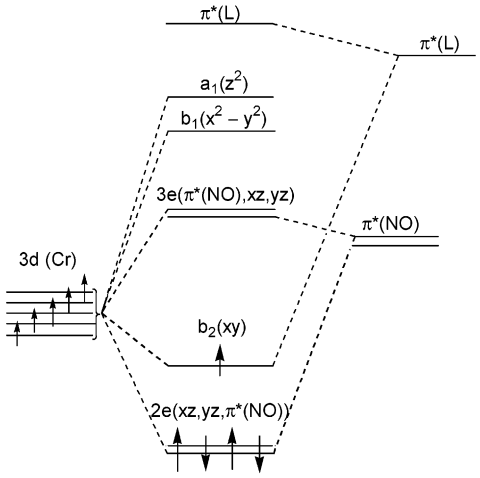

Figure 6. General molecular orbital scheme for octahedral $Cr(NO)L_5$ complexes.[8,20]

1). The importance of π-mixing of p and d orbitals on relaxing the selection rules is also highlighted by the much greater intensities of band B in $[Cr(CN)_6]^{3-}$ and $[Cr(NCS)_6]^{3-}$ compared with $[Cr(OH_2)_6]^{3+}$ and $[Cr(acac)_3]$ (Figure 1). Thus, XANES spectroscopy of Cr−NO complexes with O-, N-, or C-donor ligands provides the first direct measurement of the degree of π-back-bonding in such complexes.

Acknowledgment. Financial support of this work was provided by an Australian Research Council (ARC) grant (to P.A.L.), and by an ARC RIEFP grant for the fluorescence detector at Australian National Beamline Facility (ANBF). X-ray absorption spectroscopy was performed at the ANBF with support from the Australian Synchrotron Research Program, which is funded by the Commonwealth of Australia under the Major National Research Facilities program. The authors thank Dr. Garry Foran (ANBF) and Ms. Jade Aitken (University of Sydney) for the help in XAS data collection, Dr. Andrew Berry (Australian National University) for providing unpublished results of his work, Dr. Marina Fainerman-Melnikova (University of Sydney) for helpful discussions, and Mr. Fernando Barasoain (University of Sydney) for the synthesis of $[Cr(acac)_3]$.

Supporting Information Available: Figures showing the EPR, UV−vis, and IR spectra of the Cr−NO and Cr(III) complexes, comparison of XANES spectra of $K_3[Cr(NO)(CN)_5]$ and $K_3[Cr(CN)_6]$ at 17 K, and the structures of $[Cr(NO)(OH_2)_5]^{2+}$, optimized by MS XAFS calculations. Tables showing the results of elemental analyses, magnetic measurements, and EPR spectroscopy for the synthesized complexes. Details of MS XAFS calculations for $[Cr(NO)(OH_2)_5]^{2+}$ and *cis*- and *trans*-$[Cr(NO)(acac)_2(OH_2)]$: (i) conditions, restraints, and constraints applied to the MS XAFS models; (ii) parameters of the optimized models; and (iii) most significant scattering paths of a photoelectron for the optimized models. Details of the crystal structure of $(Ph_4P)_3[Cr(NO)(NCS)_5]\cdot 2.4(CH_3)_2CO$ as CIF data. This material is available free of charge via the Internet at http://pubs.acs.org.

IC0340480